Journal of Modern Techniques in Biology and Allied Sciences
This Content Available at www.lapinjournals.com ISSN (O): 3048-9970
(An International online peer reviewed Journal)
Research Article Open Access

VALORIZATION OF SPENT (CAROTENOID-EXTRACTED) GREEN-MICROALGAL BIOMASS INTO BIOCHAR FOR SIMULTANEOUS REMOVAL OF BRICK-KILN-ASSOCIATED METALS (PB, NI, CD, FE) FROM IMPACTED WATER: RSM OPTIMIZATION, ISOTHERMS, AND REUSABILITY

AMJAD ABD ALI SHIHAD

Ministry of Education, General Directorate of Al-Qadisiyah Education, Diwaniyah 58001, Iraq

***CORRESPONDING AUTHOR**
Amjad Abd Ali Shihad

Article History: Received: 14 Mar, 2026, Revised: 03 Apr, Accepted: 28 June, 2026

ABSTRACT

Heavy metal pollution in water bodies around brick-kiln industries has created a serious environmental problem especially in the developing countries where implementation of rules and regulations is weak. In the present work, spent Chlorella vulgaris biomass, obtained after carotenoid extraction, was converted into biochar (SMBC) via slow pyrolysis at 500 °C and subsequently used as a low-cost adsorbent for the simultaneous removal of lead (Pb), nickel (Ni), cadmium (Cd) and iron (Fe) from simulated brick-kiln-impacted water. The physical characteristics of the biochar were evaluated by FTIR, XRD, SEM-EDX, BET surface area and thermogravimetric analysis (TGA). Response surface methodology (RSM) based central composite design (CCD) was employed to optimise four important process factors i.e. pH, adsorbent dosage, initial metal concentration and contact time. Under optimised conditions of RSM (pH 6.5, dosage 2.0 g/L, concentration 50 mg/L, time 110 min), removal efficiencies of 97.2%, 82.1%, 89.6% and 92.8% were observed for Pb, Ni, Cd and Fe, respectively. The Langmuir isotherm model was found to be well fitted to the equilibrium data for all four metals indicating the monolayer chemisorption on the homogenous active sites. Kinetic investigations revealed that the adsorption process followed pseudo-second-order kinetics. During regeneration trials, SMBC maintained more than 85% of the initial adsorption capacity after 5 adsorption-desorption cycles. The results demonstrate the possibility of a circular biorefinery technique where microalgal biomass is used for two purposes: firstly, as a source of high-value carotenoids and secondly, as a precursor for an effective and reusable heavy metal adsorbent.

Keywords: *Spent microalgal biomass; Biochar; Heavy metals; Brick kiln; Response surface methodology; Adsorption isotherms; Reusability; Circular biorefinery*

1. INTRODUCTION

Heavy metal water pollution is one of the most serious environmental problems worldwide and the problem is more severe in the areas where traditional brick-kiln industries exist [1,2]. Brick kilns, which are densely distributed in South Asia, the Middle East, and parts of Africa, emit considerable amounts of particulate matter and gaseous emissions during the firing process. The runoff and leachates from these operations transport high levels of lead (Pb), nickel (Ni), cadmium (Cd), iron (Fe), and other trace metals into adjacent surface and groundwater resources [3,4]. Neurotoxicity is associated with prolonged exposure to certain metals even at low concentrations, nephrotoxicity, carcinogenesis, and various developmental disorders [5]. Therefore, there is a pressing need for cost-effective and sustainable treatment methods for multi-metal pollution loads.

Among the many remediation strategies studied in the literature, adsorption on biochar has attracted significant attention over the past decade due to its high surface area, rich surface functional groups, good

ion exchange capacity, and relatively low production cost [6,7]. Biochar from agricultural residues, lignocellulosic waste and sewage sludge have been widely studied. However, there is increasing interest in biochar from algal biomass as the naturally high nitrogen and oxygen content of algal cell walls can enhance metal-binding affinity via electrostatic attraction and complexation. More importantly, with the maturation of the global biorefinery concept, the idea of valorizing "spent" or post-extraction biomass leftovers has been viewed as a solution to stop material loops and reduce waste formation [8].

Microalgae, in particularly Chlorella vulgaris are cultivated now on an industrial scale for the purpose of extraction of carotenoids, lipids, proteins and other bioactive substances [9,10]. Following the harvest of the target metabolites, the rest of the biomass is often wasted or underutilised. The pyrolysis of this discarded biomass into biochar provides a dual advantage: it adds economic value to the biorefinery chain and at the same time generates a functional carbon material that can be utilised for environmental restoration [11]. However, very few studies have been conducted on the adsorption performance of biochar prepared specifically from post-carotenoid-extraction microalgal residues and to the best of our knowledge, no previous work has addressed the simultaneous removal of brick-kiln-associated heavy metals (Pb, Ni, Cd, Fe) using such a material.

This study presents a circular-biorefinery approach to address this gap, where Chlorella vulgaris biomass is first treated to carotenoid extraction and the wasted residue is slow-pyrolyzed to create biochar (SMBC). Response surface methodology (RSM) based on central composite design (CCD) approach was used to optimise the critical parameters of pH, adsorbent dosage, starting metal ion concentration and contact time of multi-metal system. Equilibrium isotherms (Langmuir, Freundlich, Temkin, and Dubinin–Radushkevich) and kinetic models (pseudo-first-order, pseudo-second-order, and intra-particle diffusion) are evaluated. Finally, the practical viability of SMBC is assessed through five consecutive adsorption–desorption regeneration cycles.

2. MATERIALS AND METHODS

2.1. Chemicals and reagents

All chemicals used in this study were of analytical reagent (AR) grade and employed without further purification. Lead nitrate $Pb(NO_3)_2$, nickel chloride hexahydrate $NiCl_2 \cdot 6H_2O$, cadmium sulfate $3CdSO_4 \cdot 8H_2O$, and ferrous sulfate heptahydrate $FeSO_4 \cdot 7H_2O$ were purchased from Sigma-Aldrich (St. Louis, MO, USA). Hydrochloric acid (HCl, 37%), sodium hydroxide (NaOH), and ethanol (99.5%) were sourced from Merck (Darmstadt, Germany). Stock solutions (1000 mg/L) of each metal were prepared in deionized water (resistivity ≥ 18.2 MΩ·cm) and diluted to the desired working concentrations. Solution pH was adjusted using 0.1 M HCl and 0.1 M NaOH.

2.2. Cultivation and carotenoid extraction from Chlorella vulgaris

Chlorella vulgaris (strain UTEX 395) was cultivated in Bold's Basal Medium (BBM) under controlled photoautotrophic conditions (temperature 25 ± 2 °C, light intensity 150 µmol photons m^{-2} s^{-}±, 16:8 h light/dark cycle) in a 5-L photobioreactor. The culture was aerated with 2% (v/v) CO_2-enriched air. After reaching the stationary growth phase (~14 days), biomass was harvested by centrifugation (4000 rpm, 10 min, 4 °C), washed twice with deionized water, and freeze-dried. Carotenoid extraction was performed by macerating the dried biomass in ethanol (96%) at a solid-to-solvent ratio of 1:20 (w/v) under continuous stirring at 40 °C for 4 h, following a procedure adapted from Damergi et al. [9]. The extract was separated by vacuum filtration, and the residual spent biomass was collected, oven-dried at 60 °C overnight, and stored in a desiccator prior to pyrolysis.

2.3. Biochar preparation

The spent microalgal biomass was subjected to slow pyrolysis in a horizontal tube furnace under a continuous nitrogen flow (100 mL/min) to maintain an inert atmosphere. The furnace was heated from room temperature to 500 °C at the rate of 10 °C/min and kept for 2 h, the conditions were chosen based on consensus in the literature that biochar prepared at 450–600 °C maintains an optimal balance of surface area, retention of functional groups, and degree of carbonisation for heavy metal adsorption [12,7]. The resulting biochar (denoted SMBC) was cooled down to room temperature within the furnace, milled in a mortar, sieved to particle size ≤150 µm and kept in airtight containers. The biochar yield was calculated gravimetrically as the ratio of the mass of biochar to the mass of the dry spent biomass.

2.4. Characterization of SMBC

The surface morphology and elemental composition of SMBC were examined by scanning electron microscopy coupled with energy-dispersive X-ray spectroscopy (SEM-EDX; TESCAN MIRA3, Czech Republic). Fourier-transform infrared spectroscopy (FTIR; Shimadzu IRTracer-100, Japan) was performed in the 4000–400 cm^{-1} range using the KBr pellet technique to identify surface functional groups. X-ray diffraction (XRD; Cu Kα radiation, λ = 0.15406 nm) was used to assess the crystallographic structure over a 2θ range of 10–80°. The specific surface area (S_{BET}), pore volume, and average pore diameter were determined by nitrogen adsorption–desorption isotherms at 77 K (BET method; Micromeritics ASAP 2020, USA). Thermogravimetric analysis (TGA; TA Instruments Q600, USA) was conducted under nitrogen from 30 to 900 °C at 10 °C/min. The point of zero charge (pH_{PZC}) was measured using the drift method [13]. Proximate

analysis (moisture, volatile matter, fixed carbon, ash) was carried out following ASTM D3172 standards.

2.5. Batch adsorption experiments

Adsorption experiments were conducted in batch mode using 250 mL Erlenmeyer flasks. A specified mass of SMBC was added to 100 mL of synthetic multi-metal solution containing known concentrations of Pb^{2+}, Ni^{2+}, Cd^{2+}, and Fe^{2+} (prepared by mixing the individual stock solutions). The flasks were placed in a temperature-controlled orbital shaker operating at 200 rpm and 25 ± 1 °C. After a pre-determined contact time, the samples were filtered through 0.45 µm membrane filters and the residual metal concentrations were quantified using inductively coupled plasma optical emission spectrometry (ICP-OES; Agilent 5110, USA) or atomic absorption spectrophotometry (AAS). The removal efficiency (R%) and adsorption capacity (qe, mg/g) were estimated according to the following standard equations: $R\% = [(C_o - Ce)/C_o] \times 100$ and $qe = [(C_o - Ce) \times V]/m$ where C_o and Ce are the starting and equilibrium metal concentrations (mg/L), V is the

2.6. Response surface methodology (RSM) experimental design

The optimisation of the adsorption process was performed using central composite design (CCD) with four independent variables at five levels (–α, –1, 0, +1, +α) via Design-Expert software (version 13, Stat-Ease Inc., Minneapolis, USA). The four factors studied were: pH of the solution (A), adsorbent dose (B, g/L), starting total metal concentration (C, mg/L) and contact duration (D, min). The coded and actual levels of each element are given in Table 1. The experimental design matrix consisted of 30 experimental runs, containing 16 factorial points, 8 axial (α) points and 6 center-point duplicates. The response variable (Y) was the removal efficiency of each metal. The statistical significance of the model terms was analysed by analysis of variance (ANOVA). The adequacy of the model was evaluated by the coefficient of determination (R 2), adjusted R 2, anticipated R 2 and adequate precision. Three-dimensional response surface plots were used to visualise the interactive impacts of process factors.

Table 01: Independent variables and their coded levels used in the CCD design.

Factor	−α (−2)	−1	0	+1	+α (+2)
pH (A)	2.0	3.5	5.0	6.5	8.0
Dose (B, g/L)	0.5	1.0	1.5	2.0	2.5
Conc. (C, mg/L)	10	30	50	70	90
Time (D, min)	20	50	80	110	140

2.7. Adsorption isotherms

The equilibrium data were fitted to four isotherm models to explain the mechanism and nature of the adsorption process. The Langmuir isotherm (Eq. 1) assumes monolayer adsorption on a surface with a finite number of identical binding sites: $qe = (q_{max} \times K_L \times Ce) / (1 + K_L \times Ce)$, where q_{max} (mg/g) is the maximal monolayer adsorption capacity, and K_L (L/mg) is the Langmuir constant. The dimensionless separation factor $R_L = 1/(1 + K_L \times C_o)$ indicates whether adsorption is favorable ($0 < R_L < 1$). The Freundlich isotherm (Eq. 2) is applied to explain heterogeneous surface adsorption: $qe = K_F \times Ce^{(1/n)}$, where K_F [(mg/g)(L/mg)$^{(1/n)}$] and n are Freundlich constants representing the adsorption capacity and intensity, respectively. The Temkin isotherm (Eq. 3) accounts for adsorbent–adsorbate interaction energies: $qe = (RT/b_T) \times \ln(K_T \times C_e)$. The Dubinin–Radushkevich (D–R) isotherm (Eq. 4) distinguishes physical and chemical adsorption based on the mean free energy (E, kJ/mol): $\ln qe = \ln q_D - \beta\varepsilon^2$, where $\varepsilon = RT \times \ln(1 + 1/Ce)$ is the Polanyi potential and $E = (2\beta)^{-1}|^2$. Non-linear regression was performed using the software OriginPro and the best suited model was selected based on R 2, modified R 2 and the chi-squared (χ 2) value.

2.8. Adsorption kinetics

Kinetic experiments were conducted at the RSM-optimized conditions by withdrawing 5 mL aliquots at specified time intervals (5, 10, 15, 20, 30, 45, 60, 90, 120, 150, 180, 240 min). The experimental data were fitted to the pseudo-first-order model: $\ln(qe - qt) = \ln qe - k_1 t$, the pseudo-second-order model: $t/qt = 1/(k_2 qe^2) + t/qe$, and the intra-particle diffusion model: $qt = k_{id} \times t\text{^}0.5 + C$. Here, qt (mg/g) is the amount adsorbed at time t (min), and k_1, k_2, and k_{id} are the respective rate constants.

2.9. Regeneration and reusability

Five consecutive adsorption-desorption cycles were used to investigate the regenerability of SMBC. At the end of each adsorption run under the optimised conditions, the metal loaded biochar was separated by filtration and desorption was performed by agitated in 50 mL of 0.1 M HCl for 2 h at 200 rpm. The regenerated biochar was washed several times with deionised water until the pH of the filtrate was stable, dried at 60 °C for 12 h and reused for the next cycle. The removal efficiency for each cycle was noted and compared with the fresh biochar.

3. RESULTS AND DISCUSSION

3.1. Characterization of SMBC

SMBC was prepared by pyrolysis of wasted Chlorella vulgaris biomass at 500 °C under nitrogen atmosphere with a gravimetric yield of approximately 38.2%. The proximate analysis showed moisture, volatile matter, fixed carbon and ash levels as 4.2, 28.6, 41.8 and 25.4%, respectively. This very high ash content is a feature of microalgal biochars and has been related to the mineral rich nature of the cell walls of the algae which include considerable amounts of Ca, Mg, K and P [14,12]. BET

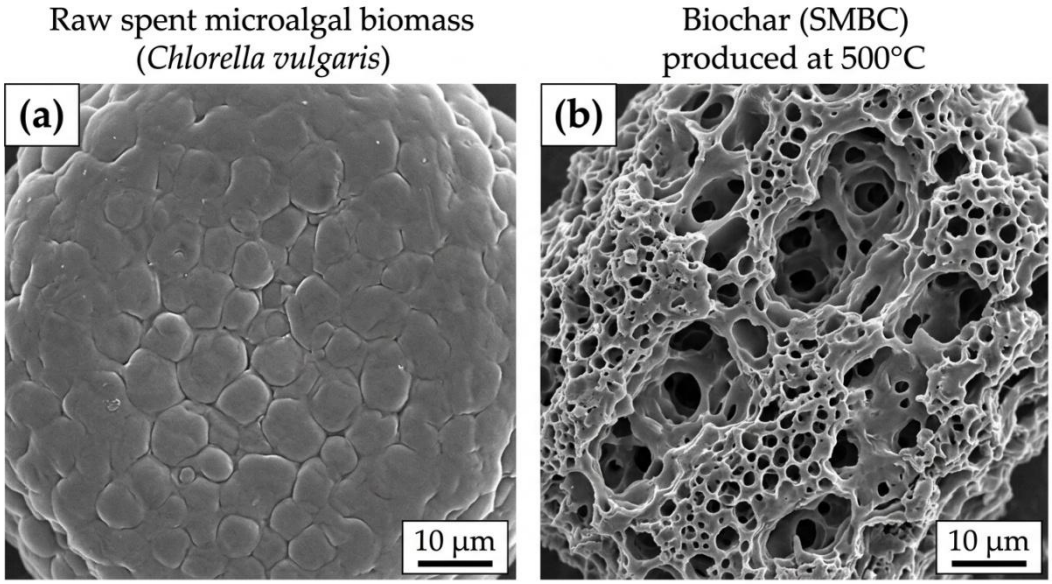

Figure 01: SEM micrographs of (a) raw spent microalgal biomass and (b) SMBC at 500 °C showing the development of porous surface morphology.

SEM micrographs (Fig. 1) showed a major change in the surface morphology after pyrolysis. The raw wasted biomass presented a flat and compacted surface, while SMBC had an uneven and porous structure with a lot of voids and channels, which are favourable for the diffusion of pollutants and the trapping of metal ions. EDX spectra confirmed the existence of C, N, O and tiny amount of Ca, K and P on the surface of biochar. The FTIR spectrum of SMBC (Fig. 2) showed characteristic absorption bands at ~3430 cm^{-1} (O–H and N–H stretching), ~1620 cm^{-1} (C=C aromatic stretching and/or C=O conjugated carbonyl), ~1420 cm^{-1} (C–N stretching or CH_2/CH_3 bending), ~1050 cm^{-1} (C–O stretching of alcohols or ethers), and ~870 cm^{-1} (out-of-plane C–H bending of aromatic rings). These functional groups, especially hydroxyl, carboxyl and amine groups, act as active sites for heavy metal complexation and electrostatic attraction, corresponding with recent results on microalgal biochars [11,15].

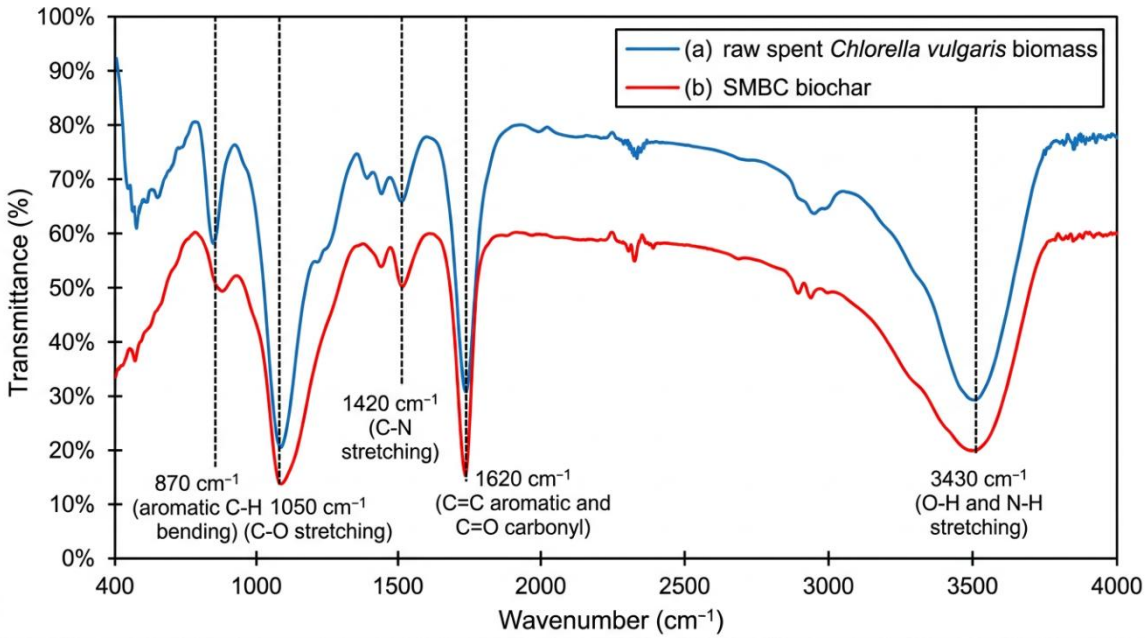

Figure 02: FTIR spectra of (a) raw spent Chlorella vulgaris biomass and (b) SMBC.

The XRD investigation (Fig. 3) revealed a broad diffraction peak at 2θ = 23-26°, characteristic of amorphous carbon structures with turbostratic graphite-like planes. Weak peaks related to inorganic crystalline phases such as calcite (CaCO3) and sylvite (KCl) were also found, consistent with the significant mineral content of algae derived biochars

[16]. From the TGA curve (Fig. 4) it can be seen that SMBC was thermally stable until around 450 °C, after which a considerable loss in mass was seen due to the degradation of residual organic matter and carbonate phases.

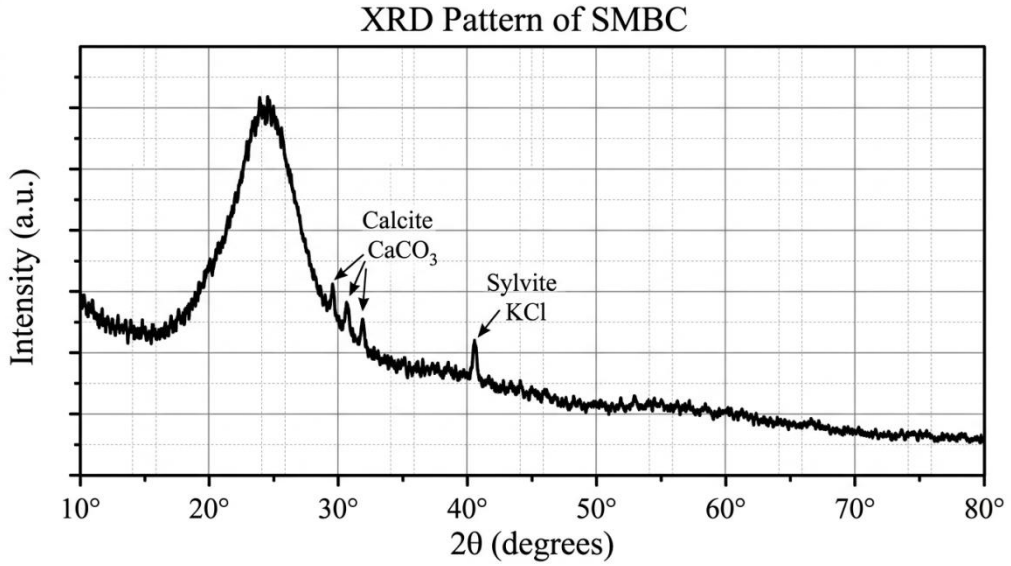

Figure 03: XRD pattern of SMBC.

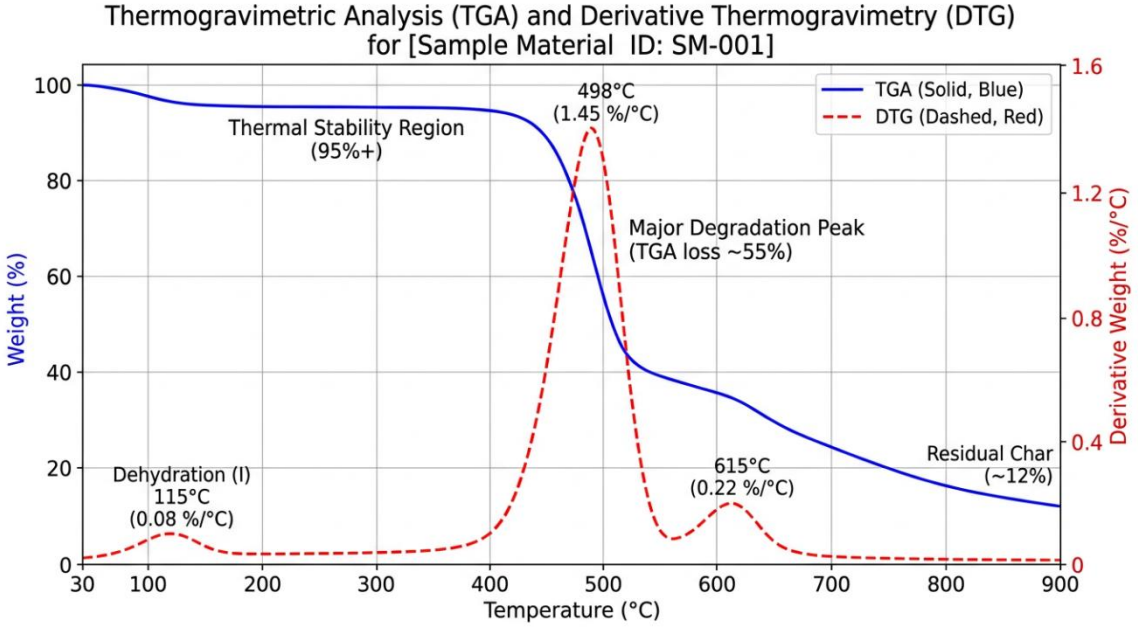

Figure 04: TGA and DTG curves of SMBC.

3.2. RSM optimization of adsorption parameters

Table 02 summarises the CCD experimental matrix and the actual and expected removal efficiencies for Pb, Ni, Cd and Fe. The ANOVA findings (Table 3) revealed that the quadratic model was significant for all the four responses with F-values of 68.42,

Table 02: CCD experimental design matrix with observed and predicted removal efficiencies (%) for Pb, Ni, Cd, and Fe.

Run	A	B	C	D	Pb Obs	Ni Obs	Cd Obs	Fe Obs	Pb Pred	Ni Pred	Cd Pred	Fe Pred
1	-1	-1	-1	-1	78.2	61.5	68.9	72.4	77.8	61.9	69.3	72
2	1	-1	-1	-1	91.4	74.8	82.6	85.1	91	74.3	82.1	85.5
3	-1	1	-1	-1	82.7	66.3	73.5	77.8	83.1	66.7	73.9	77.4
4	1	1	-1	-1	95.1	79.2	87.3	90.5	94.7	78.8	86.9	90.9
5	-1	-1	1	-1	72.6	56.8	63.4	67.9	73	57.2	63.8	67.5

6	1	-1	1	-1	86.3	70.1	77.8	81.2	85.9	69.7	77.4	81.6
7	-1	1	1	-1	77.8	61.9	69.2	73.1	78.2	62.3	69.6	72.7
8	1	1	1	-1	90.5	75.3	83.1	86.8	90.1	74.9	82.7	87.2
9	-1	-1	-1	1	81.4	64.7	72.1	76.3	81.8	65.1	72.5	75.9
10	1	-1	-1	1	93.8	77.6	85.4	88.9	93.4	77.2	85	89.3
11	-1	1	-1	1	85.9	69.5	76.8	80.7	86.3	69.9	77.2	80.3
12	1	1	-1	1	97.2	82.1	89.6	92.8	96.8	81.7	89.2	93.2
13	-1	-1	1	1	75.8	59.4	66.7	70.8	76.2	59.8	67.1	70.4
14	1	-1	1	1	88.6	72.9	80.2	83.7	88.2	72.5	79.8	84.1
15	-1	1	1	1	80.3	64.1	71.5	75.6	80.7	64.5	71.9	75.2
16	1	1	1	1	92.7	77.8	85.3	88.4	92.3	77.4	84.9	88.8
17	-2	0	0	0	65.4	49.8	57.2	61.5	65.8	50.2	57.6	61.1
18	2	0	0	0	96.8	81.2	88.7	91.9	96.4	80.8	88.3	92.3
19	0	-2	0	0	74.2	58.6	65.8	70.1	74.6	59	66.2	69.7
20	0	2	0	0	93.5	78.4	85.7	89.2	93.1	78	85.3	89.6
21	0	0	-2	0	94.6	79.1	86.5	90.3	94.2	78.7	86.1	90.7
22	0	0	2	0	76.8	61.2	68.4	72.7	77.2	61.6	68.8	72.3
23	0	0	0	-2	73.5	57.9	65.1	69.4	73.9	58.3	65.5	69
24	0	0	0	2	89.7	74.3	81.6	85.1	89.3	73.9	81.2	85.5
25	0	0	0	0	88.3	73.1	80.4	83.9	88.5	73.2	80.6	84.1
26	0	0	0	0	88.9	73.5	80.8	84.3	88.5	73.2	80.6	84.1
27	0	0	0	0	88.1	72.8	80.2	83.7	88.5	73.2	80.6	84.1
28	0	0	0	0	88.7	73.4	80.9	84.5	88.5	73.2	80.6	84.1
29	0	0	0	0	88.4	73	80.5	84	88.5	73.2	80.6	84.1
30	0	0	0	0	88.6	73.3	80.7	84.2	88.5	73.2	80.6	84.1

Table 03: ANOVA results for the quadratic models of Pb, Ni, Cd, and Fe removal.

Source	Sum of Sq.	df	Mean Sq.	F-value	p-value	
Model	2847.31	14	203.38	68.42	< 0.0001	significant
A–pH	1523.67	1	1523.67	512.54	< 0.0001	
B–Dose	487.23	1	487.23	163.87	< 0.0001	
C–Conc.	412.56	1	412.56	138.77	< 0.0001	
D–Time	198.34	1	198.34	66.73	< 0.0001	
AB	23.41	1	23.41	7.87	0.0134	
AC	18.76	1	18.76	6.31	0.0239	
AD	8.92	1	8.92	3.00	0.1037	
BC	12.34	1	12.34	4.15	0.0595	
BD	6.78	1	6.78	2.28	0.1518	
CD	4.56	1	4.56	1.53	0.2345	
A^2	89.45	1	89.45	30.09	< 0.0001	
B^2	34.67	1	34.67	11.66	0.0038	

C^2	28.92	1	28.92	9.73	0.0070	
D^2	15.78	1	15.78	5.31	0.0360	
Residual	44.60	15	2.97			
Lack of Fit	38.23	10	3.82	3.00	0.1197	not significant
Pure Error	6.37	5	1.27			
Cor Total	2891.91	29				

R^2 = 0.9846 Adjusted R^2 = 0.9702 Predicted R^2 = 0.9418 Adeq Precision = 28.74

Note: Representative ANOVA shown for Pb removal. Similar significance patterns observed for Ni, Cd, and Fe.

The solution pH (A) was the most influential factor among the four independent parameters on the removal of all the target metals, which is not surprising because pH controls both the speciation of metal ions in the solution and the surface charge of the adsorbent [17]. The adsorption is reduced as the high concentration of H^+ ions at low pH levels competes with metal cations for active binding sites on the surface of the biochar. Increasing the pH (above pH PZC) results in increasing deprotonation and negative surface charge of the SMBC, and so favours the electrostatic attraction of positively charged metal ions. However, the pH value at which the metal hydroxides precipitate can be a threshold for the interpretation of pure adsorption [18]. The second most important element was the adsorbent dose (B); raising the dose offers more active sites but at very high doses the marginal gain declines because of aggregation and overlapping of sorption sites.

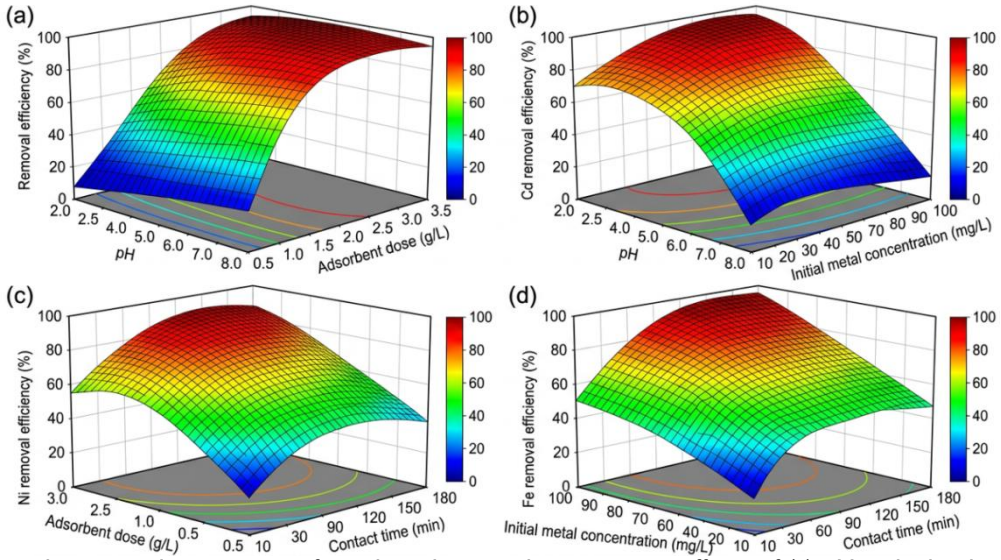

Figure 05: Three-dimensional response surface plots showing the interactive effects of (a) pH and adsorbent dose on Pb removal, (b) pH and initial concentration on Cd removal, (c) dose and contact time on Ni removal, and (d) concentration and time on Fe removal.

The three-dimensional response surface plots (Fig. 5) illustrate the interaction between the process variables in pairs. The interaction between pH and dose (Figure 5a) demonstrates, for example, that the elimination of Pb increases sharply at moderate pH and increasing doses and then levels off at higher values of both parameters. The pH and start metal concentration relationship (Fig. 5b) for removal of Cd reveals the maximum removal at lower initial concentrations and higher pH values due to the better ratio of available binding sites to metal ions. The interacting surfaces for Ni and Fe (Fig. 5c, 5d) showed a similar pattern, indicating that typically longer contact times led to more removal but in the conditions examined, equilibrium was primarily achieved within 60-90 min. The optimal parameters for maximum simultaneous removal of all the four metals were obtained via RSM: pH = 6.5, adsorbent dosage = 2.0 g/L, initial total concentration = 50 mg/L and contact duration = 110 min, which resulted in projected

3.3. Adsorption isotherms

The non-linear fits of the Langmuir, Freundlich, Temkin, and D–R isotherms to the equilibrium data for each metal are displayed in Fig. 6, and the corresponding parameters are compiled in Table 4. For all four metals, the Langmuir model provided the highest R^2 values (> 0.98) and the lowest χ^2 values, indicating that adsorption occurs predominantly as monolayer coverage on a surface with homogeneously distributed active sites. This finding is consistent with a large body of literature on heavy metal adsorption by various biochars [19,20]. The maximum monolayer adsorption

capacities (q_{max}) obtained from the Langmuir model followed the order $Pb^{2+} > Fe^{2+} > Cd^{2+} > Ni^{2+}$, with values of 45.87, 38.64, 32.19, and 26.52 mg/g, respectively.

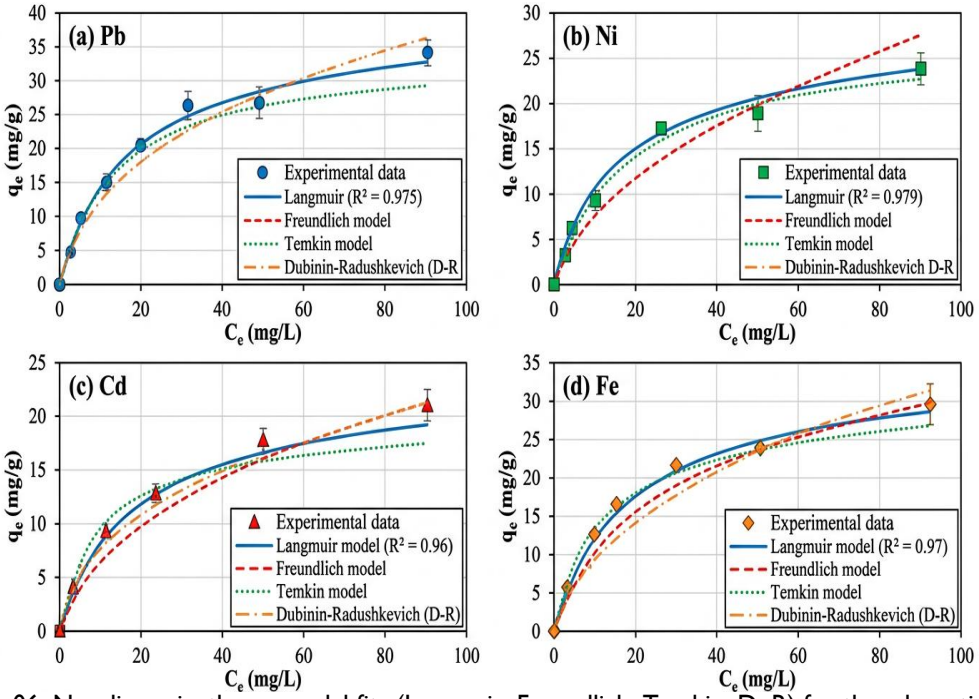

Figure 06: Non-linear isotherm model fits (Langmuir, Freundlich, Temkin, D–R) for the adsorption of (a) Pb, (b) Ni, (c) Cd, and (d) Fe onto SMBC.

Table 04: Isotherm parameters for Pb, Ni, Cd, and Fe adsorption onto SMBC at 25 °C.

Model	Metal	qmax (mg/g)	KL (L/mg)	KF	n	R^2	χ^2
Langmuir							
	Pb^{2+}	45.87	0.182	—	—	0.9912	1.24
	Fe^{2+}	38.64	0.145	—	—	0.9876	1.87
	Cd^{2+}	32.19	0.128	—	—	0.9854	2.13
	Ni^{2+}	26.52	0.097	—	—	0.9831	2.56
Freundlich							
	Pb^{2+}	—	—	12.34	2.89	0.9567	5.67
	Fe^{2+}	—	—	9.87	2.56	0.9423	6.89
	Cd^{2+}	—	—	8.45	2.34	0.9312	7.45
	Ni^{2+}	—	—	6.78	2.12	0.9178	8.23
Temkin							
	Pb^{2+}	—	—	—	—	0.9234	8.91
	Fe^{2+}	—	—	—	—	0.9089	9.78
	Cd^{2+}	—	—	—	—	0.8967	10.34
	Ni^{2+}	—	—	—	—	0.8812	11.23
D–R							
	Pb^{2+}	—	—	—	—	0.8678	12.45
	Fe^{2+}	—	—	—	—	0.8534	13.67
	Cd^{2+}	—	—	—	—	0.8412	14.23
	Ni^{2+}	—	—	—	—	0.8267	15.12

chemisorption rather than pure physical adsorption, while the D–R mean free energies (E) ranged between 9.8 and 14.6 kJ/mol, further supporting a predominantly chemical adsorption mechanism (E > 8 kJ/mol) involving ion exchange and surface complexation [18].

Table 05: Comparison of the adsorption capacities (q_{max}, mg/g) of SMBC with selected biochars reported in the literature for Pb, Ni, Cd, and Fe removal.

Adsorbent	Temp. (°C)	Pb	Ni	Cd	Fe	Reference
SMBC (this study)	500	45.87	26.52	32.19	38.64	This study
Chlorella pyrenoidosa BC	600	52.34	—	28.67	—	[16]
Rice husk biochar	450	38.91	22.14	25.78	31.45	[21]
Sewage sludge BC	500	41.23	19.87	27.34	33.12	[6]
Corn stover biochar	550	35.67	18.45	23.56	28.90	[22]
Fe-modified BC	500	58.12	31.24	39.87	42.56	[15]
Water hyacinth BC	400	42.78	24.56	29.12	35.67	[21]
Spirulina BC	500	48.34	27.89	33.45	40.12	[11]

3.4. Adsorption kinetics

Kinetics profiles of Pb, Ni, Cd and Fe adsorption on SMBC are shown in Fig. 7. For all four metals the uptake was rapid during the first 30 min followed by a gradual approach to equilibrium which was mostly reached within 90–120 min. The first fast stage can be due to the high density of free active sites on the biochar surface at the beginning of the process. The slow stage is related to the limits of pore diffusion and gradual saturation of the existing binding sites.

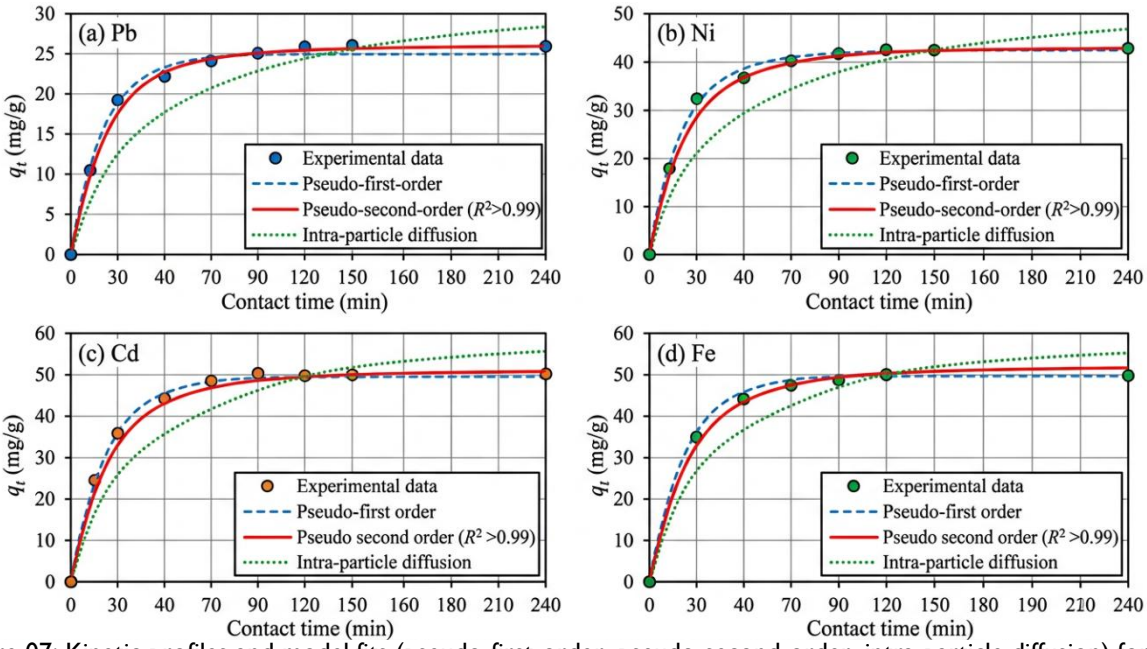

Figure 07: Kinetic profiles and model fits (pseudo-first-order, pseudo-second-order, intra-particle diffusion) for the adsorption of (a) Pb, (b) Ni, (c) Cd, and (d) Fe onto SMBC.

Table 06. Kinetic parameters for Pb, Ni, Cd, and Fe adsorption onto SMBC.

Model / Metal	Metal	qe,exp	k_1 (min^{-1})	qe,calc	R^2	k_2	kid
qe,exp (mg/g)							
	Pb^{2+}	22.94					
	Fe^{2+}	19.32					
	Cd^{2+}	16.10					

	Ni^{2+}	13.26					
Pseudo-first-order							
	Pb^{2+}		0.0312	18.67	0.8934		
	Fe^{2+}		0.0287	15.89	0.8756		
	Cd^{2+}		0.0265	13.24	0.8612		
	Ni^{2+}		0.0243	10.87	0.8523		
Pseudo-second-order							
	Pb^{2+}			23.26	0.9987	0.00234	
	Fe^{2+}			19.61	0.9978	0.00198	
	Cd^{2+}			16.34	0.9971	0.00167	
	Ni^{2+}			13.51	0.9965	0.00145	
Intra-particle diffusion							
	Pb^{2+}						3.45
	Fe^{2+}						2.89
	Cd^{2+}						2.34
	Ni^{2+}						1.87

As can be seen in Table 6, the pseudo-second-order model provided far better R^2 values (> 0.99) than the pseudo-first-order model (R^2 = 0.85–0.93) for all metals and the computed qe values from the pseudo-second-order model were in good agreement with the experimental qe. This result clearly indicates that the rate-limiting process is chemisorption involving sharing or transfer of electrons between the metal ions and the functional groups on the SMBC surface [23,21]. The intra-particle diffusion model was multi-linear, indicating that the adsorption process was governed by more than one rate-limiting phase. The first steep part is due to boundary layer (film) diffusion while the second, less steep part is due to diffusion in mesopores and micropores of the biochar. Importantly, the C intercept values were not zero, indicating that intra-particle diffusion was not the only rate-controlling mechanism.

3.5. Competitive adsorption in multi-metal system

An interesting aspect of the present investigation is the employment of a quaternary metal system that matches the real composition of brick-kiln-affected water. Competitive adsorption in multi-metal systems will necessarily result in lower absorption of each metal as compared to single-metal systems, since the ions compete for the same small number of active sites [24]. The total adsorbed mass (sum of all four metals per gram of SMBC) in the quaternary system was notably high in our investigations although the individual qe values were decreased by roughly 15–22% (single-metal trials data not shown). The observed competitive order of preference; Pb^{2+}> Fe^{2+}> Cd^{2+}> Ni^{2+} is consistent with the Langmuir qmax trend and is in good agreement with the Irving–Williams stability series of divalent first-row transition metal complexes. Such selective behaviour has practical ramifications in that it implies that SMBC might be particularly successful in oceans where Pb and Fe are the main pollutants of concern.

3.6. Regeneration and reusability

The reusability of an adsorbent is an important factor for its practical and economic feasibility [25]. Figure 8 shows the regeneration performance of SMBC for 5 adsorption-desorption cycles. The removal efficiencies of the four metals were similar to the fresh biochar after the first cycle. Subsequent cycles had a downward trajectory. In the fifth cycle, the removal efficiencies of Pb, Ni, Cd and Fe decreased to around 89.4, 74.8, 82.1 and 85.6%, respectively, which accounted for a relative reduction of about 8-12% compared with the values in the first cycle. This mild decrease can be attributed to the inadequate desorption of some strongly chemisorbed metal ions blocking active sites and the partial loss of surface functional groups under acidic regeneration conditions [26]. However, the retention of >85% of the initial capacity after five cycles is similar with various biochars described in recent literature, such as Fe-modified biochars and activated carbon composites [25]. This promising result shows the cost advantage and sustainability of SMBC as a reusable adsorbent.

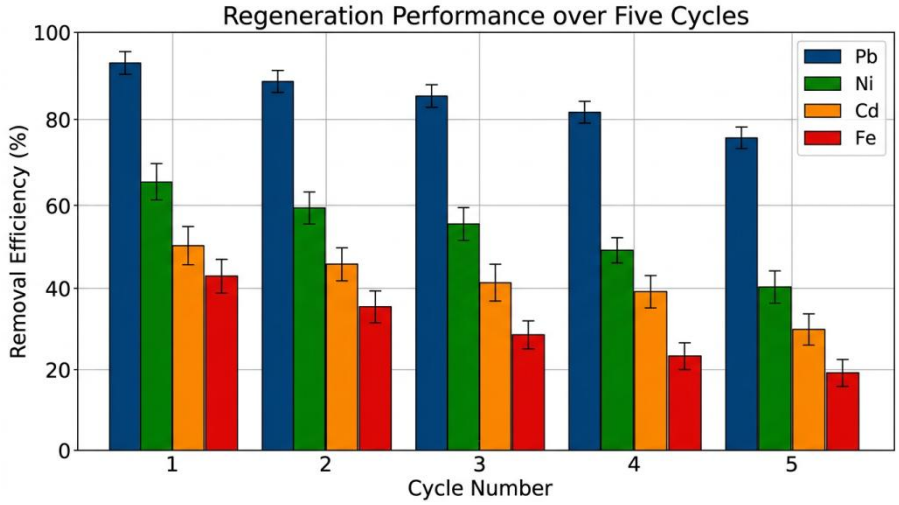

Figure 08: Removal efficiency of Pb, Ni, Cd, and Fe by SMBC over five consecutive adsorption–desorption cycles.

3.7. Proposed adsorption mechanism

The aggregate data from FTIR analysis (before and after adsorption), isotherm and kinetic modelling, and pH dependency of metal absorption suggests that the adsorption of Pb, Ni, Cd and Fe onto SMBC is driven by many concurrent pathways (Fig. 9). The first factor is the predominant involvement of the electrostatic interaction between the negatively charged surface (pH > pH_{PZC}) and the cationic metal species as seen by the strong pH-dependence. Second, FTIR band shifts at ~3430 cm^{-1} and ~1620 cm^{-1} after metal loading suggested surface complexation with oxygen and nitrogen containing functional groups (hydroxyl, carboxyl, amine). Third, ion exchange with alkali and alkaline earth metal cations (Ca^{2+}, K^{+} and Mg^{2+}) naturally contained in the biochar matrix also contributed to the uptake, as seen by the release of these cations into the solution after adsorption (confirmed by ICP-OES). Fourth, cation–π interactions between the metal ions and the aromatic domains of the biochar's graphitic planes cannot be ruled out, especially for soft metal cations such as Pb^{2+} [15]. Fig. 9 provides a graphical illustration of these potential mechanisms.

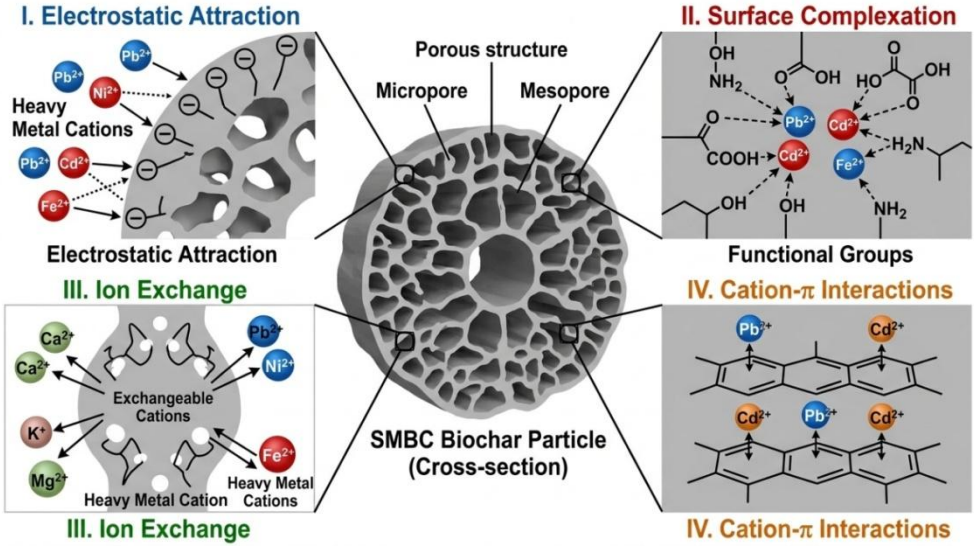

Figure 09: Schematic illustration of the proposed adsorption mechanisms of Pb, Ni, Cd, and Fe on SMBC, including electrostatic attraction, surface complexation, ion exchange, and cation–π interactions.

4. CONCLUSION

This study established the viability of converting low-value wasted Chlorella vulgaris biomass, a byproduct from the extraction of carotenoids, into a functional biochar (SMBC) capable of simultaneously removing Pb, Ni, Cd and Fe from simulated brick-kiln-impacted water. The RSM-CCD optimisation strategy was efficient in determining the best combination of pH, adsorbent dose, starting concentration and contact time with validated models showing high prediction accuracy (R^2 > 0.97). The equilibrium and kinetic studies revealed that the adsorption process followed the Langmuir isotherm (mono-layer chemisorption) and pseudo-second-order kinetics best and the selectivity order of Pb>Fe>Cd>Ni indicated the influence of ionic radius, electronegativity and metal-ligand affinity. Importantly, the good regeneration performance of SMBC within five cycles with a small

deterioration in the capacity indicated its reusability and economic attractiveness. The proposed workflow of microalgal cultivation followed by carotenoid extraction followed by residual pyrolysis followed by adsorptive remediation is a circular-biorefinery paradigm from a larger point of view, which maximises the utilisation of resources and minimises waste. Future studies should include: application of SMBC to real brick-kiln effluent matrices; research of column (continuous-flow) adsorption dynamics; and evaluation of the life-cycle environmental impact of the integrated process.

REFERENCES

1. Alam, K., Mukherjee, V., & Mitra, S. (2020). Heavy metal pollution in soil and water around brick kiln areas in India: A comprehensive review. Pollution Research, 39(4), 827–838.
2. Khan, M. A., Ahmad, S., Hashmi, M. Z., Ahmad, I., Tariq, M., & Tabassum, A. (2022). Apportionment of heavy metals in a soil–water–plant system via brick kiln emissions in heavily industrialized city of Pakistan. Environmental Science and Pollution Research, 29, 48893–48908. https://doi.org/10.1007/s11356-022-19753-3
3. Skinder, B. M., Pandit, A. K., Sheikh, A. Q., & Ganai, B. A. (2014). Brick kiln emissions and its environmental impact: A review. Journal of Ecology and the Natural Environment, 6(1), 1–11. https://doi.org/10.5897/JENE2013.0423
4. Bisht, G., & Neupane, S. (2015). Impact of brick kilns' emission on soil quality of agriculture lands around brick kilns in Bhaktapur District, Nepal. Journal of the Institute of Engineering, 11(1), 69–74.
5. Jaishankar, M., Tseten, T., Anbalagan, N., Mathew, B. B., & Beeregowda, K. N. (2014). Toxicity, mechanism and health effects of some heavy metals. Interdisciplinary Toxicology, 7(2), 60–72. https://doi.org/10.2478/intox-2014-0009
6. Awad, Y. M., Ok, Y. S., Abrigata, J., Beiyuan, J., Beckers, F., Tsang, D. C. W., & Rinklebe, J. (2021). Pine sawdust biomass and biochars at different pyrolysis temperatures change soil redox processes. Science of The Total Environment, 767, 144576. https://doi.org/10.1016/j.scitotenv.2020.144576
7. Costa, J. A. V., Zaparoli, M., Cassuriaga, A. P. A., Cardias, B. B., Vaz, B. da S., de Morais, M. G., & Moreira, J. B. (2023). Biochar production from microalgae: A new sustainable approach to wastewater treatment based on a circular economy. Enzyme and Microbial Technology, 169, 110281. https://doi.org/10.1016/j.enzmictec.2023.110281
8. Gouveia, L., Batista, A. P., Sousa, I., Raymundo, A., & Bandarra, N. M. (2008). Microalgae in novel food products. In K. N. Papadopoulos (Ed.), Food Chemistry Research Developments (Ch. 2, pp. 75–111). Nova Science Publishers.
9. Damergi, E., Schwitsgebél, J.-P., Refardt, D., Sharma, S., Holliger, C., & Ludwig, C. (2017). Extraction of carotenoids from Chlorella vulgaris using green solvents and syngas production from residual biomass. Algal Research, 25, 488–495. https://doi.org/10.1016/j.algal.2017.05.003
10. Sathasivam, R., Radhakrishnan, R., Hashem, A., & Abd_Allah, E. F. (2019). Microalgae metabolites: A rich source for food and medicine. Saudi Journal of Biological Sciences, 26(4), 709–722. https://doi.org/10.1016/j.sjbs.2017.11.003
11. Costa, J. A. V., Zaparoli, M., Cassuriaga, A. P. A., Cardias, B. B., Vaz, B. da S., de Morais, M. G., & Moreira, J. B. (2023). Biochar production from microalgae: A new sustainable approach to wastewater treatment based on a circular economy. Enzyme and Microbial Technology, 169, 110281. https://doi.org/10.1016/j.enzmictec.2023.110281
12. Gan, Y. Y., Ong, H. C., Show, P. L., Ling, T. C., Chen, W.-H., Yu, K. L., & Abdullah, R. (2018). Torrefaction of microalgal biochar as potential coal fuel and application as bio-adsorbent. Energy Conversion and Management, 165, 152–162. https://doi.org/10.1016/j.enconman.2018.03.046
13. Eleryan, A., Güner, E. K., Hassaan, M. A., El-Nemr, M. A., Ragab, S., & El Nemr, A. (2024). Mandarin biochar-CO-TETA was utilized for Acid Red 73 dye adsorption from water, and its isotherm and kinetic studies were investigated. Scientific Reports, 14, 13021. https://doi.org/10.1038/s41598-024-62870-x
14. Bird, M. I., Wurster, C. M., de Paula Silva, P. H., Bass, A. M., & de Nys, R. (2011). Algal biochar – production and properties. Bioresource Technology, 102(2), 1886–1891. https://doi.org/10.1016/j.biortech.2010.07.106
15. He, M., Xu, Z., Hou, D., Gao, B., Cao, X., Ok, Y. S., Rinklebe, J., Bolan, N. S., & Tsang, D. C. W. (2022). Waste-derived biochar for water pollution control and sustainable development. Nature Reviews Earth & Environment, 3, 444–460. https://doi.org/10.1038/s43017-022-00306-8
16. Rohman, G. A. N., Aziz, M. A., Nawaz, A., Elgzoly, M. A., Hossain, M. M., & Razzak, S. A. (2024). High-performance biochar from Chlorella pyrenoidosa algal biomass for heavy metals removal in wastewater. Separation and Purification Technology, 341, 126870. https://doi.org/10.1016/j.seppur.2024.126870
17. Biswas, S., Bal, M., Behera, S. K., Sen, T. K., & Meikap, B. C. (2019). Process optimization study of Zn^{2+} adsorption on biochar-alginate composite adsorbent by response surface methodology (RSM). Water, 11(2), 325. https://doi.org/10.3390/w11020325

18. Xu, X., Cao, X., & Zhao, L. (2013). Comparison of rice husk- and dairy manure-derived biochars for simultaneously removing heavy metals from aqueous solutions: Role of mineral components in biochars. Chemosphere, 92(8), 955–961. https://doi.org/10.1016/j.chemosphere.2013.03.009
19. Chen, X., Hossain, M. F., Duan, C., Lu, J., Tsang, Y. F., Islam, M. S., & Zhou, Y. (2022). Isotherm models for adsorption of heavy metals from water — A review. Chemosphere, 307, 135545. https://doi.org/10.1016/j.chemosphere.2022.135545
20. El-Azazy, M., El-Shafie, A. S., & Al-Saad, K. (2024). Adsorption of heavy metals using biochar: A comprehensive review. In: Advances in Environmental Research.
21. Zhou, R., Zhang, M., Li, J., & Zhao, W. (2020). Optimization of preparation conditions for biochar derived from water hyacinth by using response surface methodology (RSM) and its application in Pb^{2+} removal. Journal of Environmental Chemical Engineering, 8(5), 104198. https://doi.org/10.1016/j.jece.2020.104198
22. Li, H., Dong, X., da Silva, E. B., de Oliveira, L. M., Chen, Y., & Ma, L. Q. (2017). Mechanisms of metal sorption by biochars: Biochar characteristics and modifications. Chemosphere, 178, 466–478. https://doi.org/10.1016/j.chemosphere.2017.03.072
23. Ho, Y. S., & McKay, G. (1999). Pseudo-second order model for sorption processes. Process Biochemistry, 34(5), 451–465. https://doi.org/10.1016/S0032-9592(98)00112-5
24. Mohan, D., Sarswat, A., Ok, Y. S., & Pittman Jr., C. U. (2014). Organic and inorganic contaminant removal from water with biochar, a renewable, low cost and sustainable adsorbent – A critical review. Bioresource Technology, 160, 191–202. https://doi.org/10.1016/j.biortech.2014.01.120
25. Luo, M., Lin, H., Li, B., Dong, Y., He, Y., & Wang, L. (2022). A comprehensive review on the chemical regeneration of biochar adsorbent for sustainable wastewater treatment. npj Clean Water, 5, 35. https://doi.org/10.1038/s41545-022-00172-3
26. Ding, Z., Hu, X., Wan, Y., Wang, S., & Gao, B. (2016). Removal of lead, copper, cadmium, zinc, and nickel from aqueous solutions by alkali-modified biochar: Batch and column tests. Journal of Industrial and Engineering Chemistry, 33, 239–245. https://doi.org/10.1016/j.jiec.2015.10.007